

# Influence of liquid crystalline formation on the phase behavior of side-chain liquid crystalline block copolymers



Liangliang Ji, Xiaofang Chen, Yanhong Wu, Xiaoming Yang<sup>\*</sup>, Yingfeng Tu<sup>\*</sup>

Suzhou Key Laboratory of Macromolecular Design and Precision Synthesis, Jiangsu Key Laboratory of Advanced Functional Polymer Design and Application, College of Chemistry, Chemical Engineering and Materials Science, Soochow University, Suzhou 215123, China

## ARTICLE INFO

### Article history:

Received 1 November 2014  
Received in revised form  
23 January 2015  
Accepted 29 January 2015  
Available online 9 February 2015

### Keywords:

Liquid crystalline block copolymers  
Self-assembly  
Surface morphology

## ABSTRACT

A series of narrowly distributed diblock copolymers composed of amorphous components and side-chain liquid crystalline (LC) polymer, poly (butyl acrylate)-*block*-poly [8-(4-cyano-4'-biphenyl)-1-octanoyl acrylate] (PBA-*b*-PCBOA), with side-chain LC block weight fraction ( $f_{w,PCBOA}$ ) ranging from 25% to 87%, were synthesized by atom transfer radical polymerization (ATRP). Their thermal property, LC behavior, bulk phase behavior and thin film morphology were studied by differential scanning calorimetry (DSC), polarizing optical microscope (POM), small-angle X-ray scattering (SAXS) techniques and atomic force microscopy (AFM), respectively. The results show the diblock copolymers with different composition could present sphere, lamellar and cylinder morphologies before the order–disorder transition. As the mesogen units self-organize to form smectic phase, the lamellar morphology dominates during the majority LC block weight fraction range ( $f_{w,PCBOA} = 46\%–77\%$ ) to minimized the surface energy. Interestingly, for spin-coated thin film, the lamella phase separation size decreased with increasing annealing time. For the copolymer with  $f_{w,PCBOA}$  of 67%, a thermoreversible order–order transition (OOT) and lamella to lamella/modified layer (L/ML), were observed.

© 2015 Elsevier Ltd. All rights reserved.

## 1. Introduction

The bulk phase separation of block copolymers (BCPs) has been investigated intensively in the last decades because of the diverse nanostructures formed, such as spheres, cylinders, and lamellas [1–5]. The self-assembled morphologies are determined by the volume fraction ( $f$ ) of the individual block and  $\chi N$ , where  $\chi$  is the Flory–Huggins interaction parameter and  $N$  is the total degree of polymerization of the copolymers [6–8]. Among BCPs, liquid crystalline block copolymers (LCBCPs) have been extensively studied in recent years owing to their organization at different scales to yield structure-within-structure hierarchical structures and offering an opportunity to investigate the interplay between the molecular level LC orders and the microphase-separated domain morphologies [9,10]. As a result of the strong phase separation between the LC blocks to coil blocks, the asymmetry phase diagram and new morphologies have been observed [11–13]. In addition, hierarchical structures with several 10 nm of phase-

separation structure and about 1 nm of LC mesogen structure are formed in LCBCPs [14–18]. For example, the LC phase transitions of the LC blocks can trigger order–disorder transitions (ODTs) or order–order transitions (OOTs) of the nanophase-separated structures of BCPs, due to the cooperatively orientation in a preferred direction [19–21]. The OOT corresponds to a thermotropic phase change in microphase morphology induced simply by the change in annealing temperatures. Sanger et al. reported an OOT in the morphology of a block copolymer accompanied by the loss of the anisotropic phase structure above the isotropization temperature of the LC block [19]. In this study, the OOT of LCBCPs triggered by LC blocks is investigated.

It has been reported that the region of stability of the lamellar phase is enhanced in certain side-chain LCBCPs compared to coil–coil diblocks, where it is shifted by composition range [22]. For BCPs with side-chain LC and amorphous blocks, at high volume fractions of the LC block, hexagonally packed cylinders by amorphous blocks have been observed inside a continuous matrix of the blocks with the LC side groups [23,24]. With decreased volume fraction of the LC block, lamellar structures, and LC cylindrical microdomains with the mesogens parallel to the axis of cylinders have been observed [25]. The thermal–dynamic stable phase of

<sup>\*</sup> Corresponding authors.

E-mail addresses: [yangxiaoming@suda.edu.cn](mailto:yangxiaoming@suda.edu.cn) (X. Yang), [tuyingfeng@suda.edu.cn](mailto:tuyingfeng@suda.edu.cn) (Y. Tu).

BCPs with side-chain LC and amorphous blocks have attracted great research interests since the orientation of the LC mesogen groups will exhibit rich order structures and show strong interplay between orders of different scales. Potemkin et al. developed a theory of microphase separation in a melt of smectic BCPs with side-chain LC and amorphous blocks using the strong segregation approximation. They predicted thermodynamic stability of two types of cylindrical structures having amorphous and liquid crystalline cores, and four types of lamellar structures [26]. Hammond et al. used the side-chain LC content as a tool to tune the interfacial interactions of the LC mesophase, which allows for the orientation and ordering of the morphologies to be manipulated, includes perpendicular and parallel cylinder morphologies [27]. On the other hand, the phase-separation structure affected by the dynamic process of LC formation on microphase separation morphology is important and need further investigation.

To study the influences of LC formation on BCPs self-assembly at different annealing conditions, herein we report the controllable synthesis of a series of the diblock copolymers composed of amorphous components and side-chain LC, poly (butyl acrylate)-*block*-poly [8-(4-cyano-4'-biphenyl)-1-octanoyl acrylate] (PBA-*b*-PCBOA). PBA was selected as amorphous block component while PCBOA as side-chain liquid crystalline block due to their relatively low  $T_{gs}$ , which enables the observation of phase transitions near room temperature (RT). The thermal properties and LC behaviors of these block copolymers as a function of weight fraction of LC blocks were investigated by differential scanning calorimetry (DSC) and polarizing optical microscope (POM), while the phase behaviors and surface morphologies were studied by small angle X-ray scattering (SAXS) and atomic force microscopy (AFM).

## 2. Experimental section

### 2.1. Materials

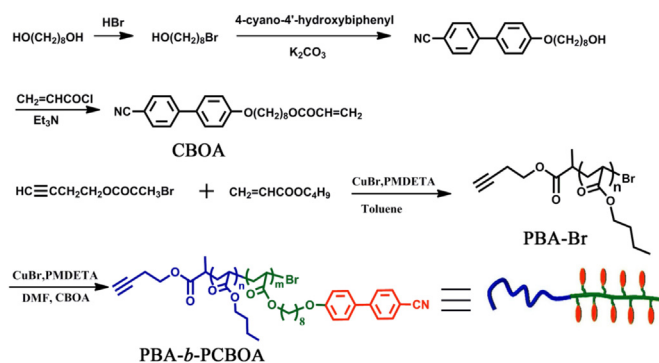
n-Butyl acrylate (BA) (Sigma–Aldrich Chemical Co.) was purified by washing with 5% sodium hydroxide solution, then with distilled water, dried over anhydrous sodium sulfate overnight, and distilled at reduced pressure over  $\text{CaH}_2$  and stored in a refrigerator. CuBr (Aldrich, 98%) was washed with glacial acetic acid, ethanol and ether to remove traces of  $\text{CuBr}_2$ . 4-Cyano-4'-hydroxybiphenyl, N,N',N'',N''-pentamethyldiethylenetriamine (PMDETA), octane-1,8-diol were obtained from Aldrich and used without further purification. All other chemical reagents were purified according to standard procedures before use.

### 2.2. Synthesis of diblock copolymers

The synthesis of PBA-*b*-PCBOA diblock copolymers is shown in Scheme 1, using sequential ATRP. The LC monomer CBOA was synthesized according to the procedure reported by Kasko et al. [28,29]. Detailed information on the synthesis and characterization is given in the Supporting information (see Fig. S1 and S2).

### 2.3. Characterization

The gel permeation chromatography (GPC) measurements were performed on a modular system comprising a Waters 1515 pump, Waters 717 plus autosampler, and 2414 refractive index detector with three 300 mm (length)  $\times$  7.5 mm (inner diameter) columns with a particle size of 5  $\mu\text{m}$  (PL gel mixed-C, Polymer Laboratories). THF was used as an eluent at a flow rate of 0.60 mL/min at 35 °C. Calibration was made against standard monodisperse linear poly-methyl methacrylate (PMMA).



**Scheme 1.** The synthetic route of the side-chain LC monomer and the diblock copolymers by ATRP.

The  $^1\text{H}$  NMR spectrum was recorded on an INOVA 400 MHz nuclear magnetic resonance instrument using  $\text{CDCl}_3$  as the solvent and tetramethylsilane (TMS) as the internal standard, with the solution concentration of 0.01 g/mL.

DSC analysis was performed using a TA Q100 instrument under a nitrogen atmosphere over a temperature range  $-20$ – $180$  °C with a scanning rate of  $10$  °C  $\text{min}^{-1}$ . The first cooling and second heating scans were used to determine the glass transition and liquid crystalline transition peaks. Typically, about 5 mg of the powdered sample was encapsulated in a sealed aluminum pan with an identical empty pan as the reference.

The phase transitions and LC textures were also investigated by POM (Olympus Corporation, BX51-P), which was coupled with a computer-controlled video camera. A dual hot stage (Linkam THMS600) was used for controlling the temperature.

SAXS measurements were performed at an X-ray scattering instrument (SAXSess  $\text{mc}^2$ , Anton Paar) equipped with line collimation and a 2200 W sealed-tube X-ray generator (Cu- $K\alpha$ ,  $\lambda = 0.154$  nm). Before measurement, samples were annealed under vacuum for 72 h at 80 °C to have good phase segregation. Samples were kept under vacuum during irradiation, and the irradiation time was 20 min at certain temperature, while imaging plate (IP) was used to record the scattering pattern. Silver behenate was used as the calibration substance to calibrate the peak positions. Anton Paar TCS 300 ( $20$  °C– $300$  °C) was used as temperature control unit conjunction with SAXSess  $\text{mc}^2$  to study the molecular arrangement at various temperatures, with a 5 min pre-equilibration delay prior to data collection at a given temperature (typical exposure time  $\sim 1$  s). The scattering vector was defined as  $q = (4\pi/\lambda) \sin(\theta/2)$ , where  $\theta$  and  $\lambda$  are the scattering angle and the wavelength of the X-ray, respectively.

The surface morphologies of thin films were measured by AFM with a tapping mode at RT (Veeco Instruments Inc., Nanoscope IV). Solutions of copolymers in toluene (4 wt%) were spin-coated at 2500 rpm onto precleaned silicon wafers. The film thickness of about 100 nm was estimated with a surface profiler. After the solvent was removed under vacuum overnight at RT, the films were annealed at a given temperature for some time and slowly cooled to RT.

## 3. Results and discussion

Up to date, as one of the controlled radical polymerization methods, ATRP has proved to be an efficient technique to synthesize different types of topological copolymers with complex macromolecular architectures and controlled molecular weights (MWs). Herein, the PBA-Br was used as macroinitiator to prepare the LCBCPs. The general synthetic procedure of the PBA-*b*-PCBOA is

**Table 1**  
Characterization data of PBA macroinitiators, LCBCPs and PCBOA.

Sample	Sample	$M_{n,GPC}^a$	$M_{n,NMR}^b$	$M_w/M_n^a$	$f_{w,PCBOA}(\%)^c$
	PBA <sub>69</sub>	$8.80 \times 10^3$		1.12	
BC-25	PBA <sub>69</sub> - <i>b</i> -PCBOA <sub>8</sub>	$9.50 \times 10^3$	$1.18 \times 10^4$	1.32	25.5
BC-33	PBA <sub>69</sub> - <i>b</i> -PCBOA <sub>12</sub>	$9.60 \times 10^3$	$1.33 \times 10^4$	1.29	33.9
BC-46	PBA <sub>69</sub> - <i>b</i> -PCBOA <sub>20</sub>	$1.02 \times 10^4$	$1.63 \times 10^4$	1.32	46.1
BC-57	PBA <sub>69</sub> - <i>b</i> -PCBOA <sub>32</sub>	$1.07 \times 10^4$	$2.09 \times 10^4$	1.33	57.8
	PBA <sub>31</sub>	$4.00 \times 10^3$		1.10	
BC-67	PBA <sub>31</sub> - <i>b</i> -PCBOA <sub>22</sub>	$9.60 \times 10^3$	$1.23 \times 10^4$	1.29	67.3
BC-77	PBA <sub>31</sub> - <i>b</i> -PCBOA <sub>36</sub>	$9.90 \times 10^3$	$1.75 \times 10^4$	1.28	77.6
BC-80	PBA <sub>31</sub> - <i>b</i> -PCBOA <sub>42</sub>	$1.01 \times 10^4$	$1.98 \times 10^4$	1.30	80.1
BC-87	PBA <sub>31</sub> - <i>b</i> -PCBOA <sub>72</sub>	$1.12 \times 10^4$	$3.11 \times 10^4$	1.28	87.3
	PCBOA	$7.90 \times 10^3$		1.25	100

<sup>a</sup> Molecular weights (g/mol) and their distribution  $M_w/M_n$  were evaluated by GPC with poly(methyl methacrylate) as standards.

<sup>b</sup> Number average molecular weights (g/mol) of the LC block were evaluated by <sup>1</sup>H NMR.

<sup>c</sup> Data in parentheses are block weight ratios of PCBOA as calculated by corresponding degree of polymerization.

shown in Scheme 1. Two types of macroinitiator ( $M_n$  are 8800 and 4000 g/mol) were synthesized, and PBA-*b*-PCBOA copolymers were synthesized using PBA-Br as macroinitiators and CBOA as monomer. By varying the LC monomer to macroinitiator molar ratio ( $[M]/[I]$ ) from 50/1 to 100/1 and polymerization time, a series of LCBCPs with different composition were obtained (shown in Table 1).

The chain-end estimation method by <sup>1</sup>H NMR to determine the number-average molecular weights of polymers is well established [30–34]. The detailed procedure is shown in the supporting information (Fig. S2). The characteristics data of the diblock copolymers are summarized in Table 1. Hereafter, BC-*x* will be used to represent LCBCPs, where B represents PBA, C represents PCBOA and *x* represents the weight percentage (wt%) of LC block in the copolymers.

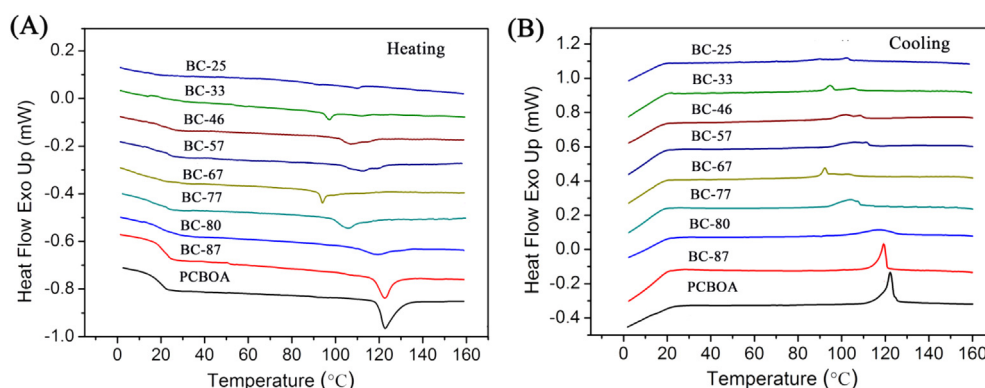
The successful preparation of a series of well-defined PBA-*b*-PCBOA copolymers with LC weight fraction ( $f_{w,PCBOA}$ ) ranging from 25% to 87% offers an ideal platform for systematically investigation of the thermal behaviors and the self-assembled suprastructures of the block copolymers.

Fig. 1 depicts a set of DSC traces for the LC homopolymer and the diblock copolymers recorded upon the second heating (A) and the first cooling (B) runs at a rate of 10 °C/min. All the samples investigated exhibited quite good reproducible thermograms in the DSC measurements. For homopolymer, two transition temperatures are observed in the DSC thermogram as follows: 22.2 °C and 123.5 °C, which are assigned to the  $T_g$  and the isotropization transition temperature ( $T_{iso}$ ) respectively [33,34].

In general, for all the sets of copolymers, the DSC curves also exhibit two transition peaks, similar to that of the homopolymer. It should be noted that the  $T_{iso}$ s of all PBA-*b*-PCBOA copolymers are lower than that of the PCBOA homopolymer, similar to other reports about the LCBCPs [35,36]. In two series of samples respectively, the  $T_{iso}$ s decrease with the decrease of LC content. But in the different series, BC-57 has higher  $T_{iso}$  than BC-67. This is because of the higher degree of polymerization of LC block in BC-57 (PBA<sub>69</sub>-*b*-PCBOA<sub>32</sub>) than in BC-67 (PBA<sub>31</sub>-*b*-PCBOA<sub>22</sub>). The isotropization transition peaks of the LCBCPs are much broader than that of the LC homopolymer. This observation might be related to a relatively poorly defined interface between the smectic blocks and the amorphous blocks, where the amorphous blocks play as “impurities” toward the smectic mesophase. Upon heating, the two blocks become more incompatible and the poorly ordered LC interfacial area becomes larger. This also results in the wide isotropization transition range observed in the DSC curve and the depression of the isotropization temperature related to the LC homopolymer. Higher LC content in the LCBCPs increases the enthalpy of LC isotropization transitions: for example, the isotropization transitions are more pronounced in BC-87 as compared to BC-80.

The individual mesomorphic properties of the homopolymer and copolymers respectively were examined by POM (Fig. 2). The focal conic texture, which belongs to typical SmA phase, was observed for homopolymer. The similar texture was also found by others [37,38]. For the PBA-*b*-PCBOA, the mesophases seem to be preserved in the LC block, as suggested by the DSC curves where the same number of peaks was detected. Also in the POM photographs, PBA-*b*-PCBOA samples show birefringence texture originating from LC phase. It's interesting that a defective focal conic texture is formed for BC-87, according to high LC weight fraction. Otherwise, the textures of the other PBA-*b*-PCBOA samples are poorly developed. For example, the sample BC-46 shows obvious birefringence but obscure texture. Furthermore, BC-25 shows both low birefringence. The birefringence in the LC phase decreases with decreasing LC weight fraction, indicating that the LC mesophase becomes less organized due to broken textures originating from less LC content and phase separation. Other samples' POM pictures are shown in Fig. S3. The destabilization of smectic phases observed in LCBCPs may result from an entropic frustration arising from confinement effect of conformationally asymmetric diblocks [39].

The morphology of the bulk films was investigated with 1D SAXS, as shown in Fig. 3. All samples were annealed in vacuum at 80 °C higher than their  $T_g$  values of the PCBOA blocks but lower than the  $T_{iso}$  values of the PCBOA blocks of LCBCPs. Typical SAXS profiles of all copolymers with various  $f_{w,PCBOA}$  recorded at RT are shown in Fig. 3. All the SAXS curves have peaks originating from



**Fig. 1.** DSC curves of PCBOA and PBA-*b*-PCBOA copolymers at (A) second heating and (B) first cooling with a scanning rate of 10 °C/min.

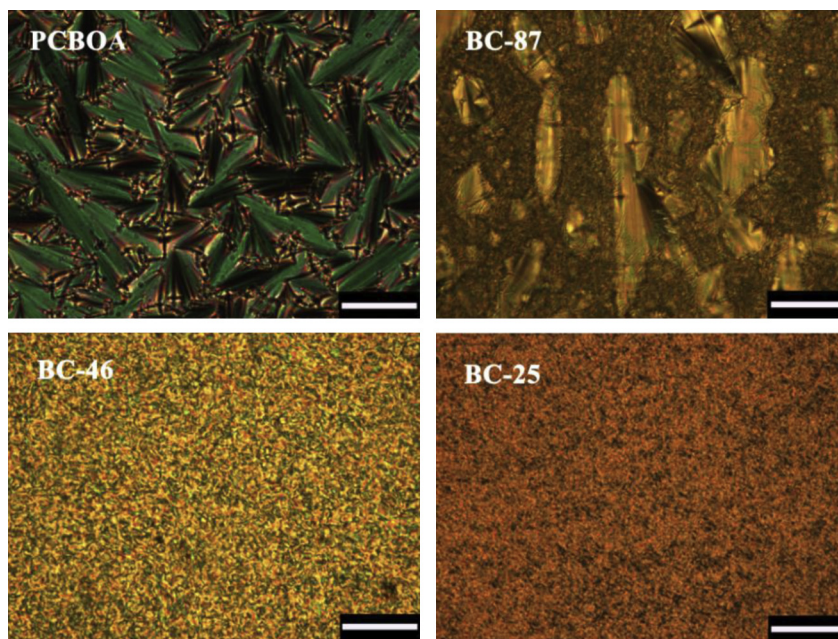


**Fig. 2.** Representative POM images of PCBOA and PBA-*b*-PCBOA copolymers under crossed polarizers. Samples were annealed from an isotropic state at a rate of 1 °C/h. The scale bar represents 50  $\mu\text{m}$ .

microphase separation structure at around  $q = 0.2\text{--}1.0 \text{ nm}^{-1}$ , although the intensity of the scattering peak for BC-87 is very weak. Similar to Shiomi's observation on their LC polymers with similar structure to ours, it's difficult to observe scattering peaks from LC mesogens [40].

The observed microphase-separated morphology is a function of the LC weight fraction. For sample BC-87, only the 1st peak is observed while the peaks at  $\sqrt{3}q$  or  $2q$  can not be found from the

SAXS curves, indicating less ordered structure formed. By combining with the results from AFM image (Fig. 4A), and also from the calculated weight fraction of LC blocks, we believe the phase separation morphology is PBA spheres in continuous PCBOA phase. The reason for the less ordered phase separation structure formed is due to the highest molecular weights of this block copolymer. The well-ordered phase separation morphology is suppressed due to increased chain entanglement and high bulk viscosity, and less

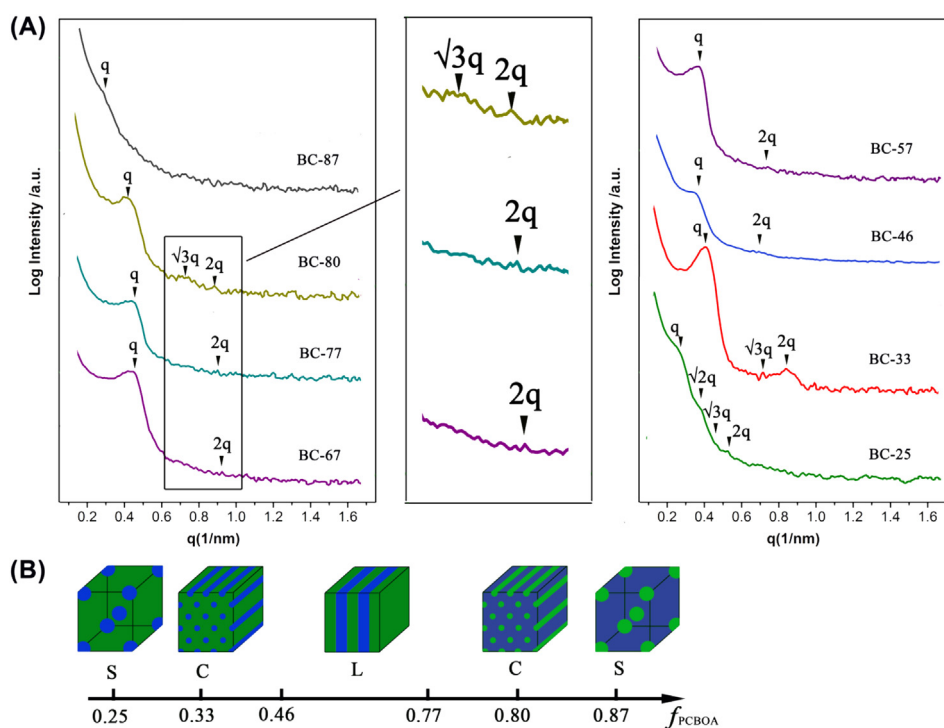


**Fig. 3.** (A) 1D SAXS of LCBCPs recorded at RT after annealing at 80 °C in vacuum for 72 h. Data are plotted as the logarithm of the relative scattered intensity  $\log I(q)$  vs the scattering factor  $q$ . (B) Experimental phase diagram of PBA-*b*-PCBOA diblock copolymers. S: sphere, C: cylinder, L: lamella.

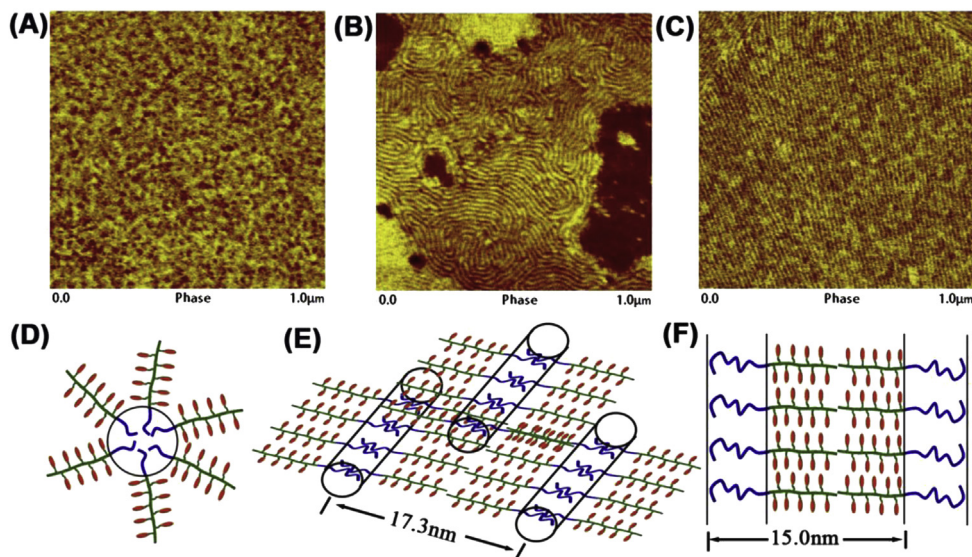


**Fig. 4.** AFM phase images of spin-coated LCBCPs films on silicon substrates after annealing at 80 °C in vacuum for 72 h. (A) BC-87, (B) BC-80, (C) BC-77. Their schematic models of the phase structure in LC state are shown as: (D) sphere, (E) cylinder, (F) lamella.

ordered structure is formed. As a result, only 1st order peak is observed from SAXS. At lower LC fractions, for BC-80, primary scattering and its higher order reflections were observed with the scattering vector in the ratio of  $1 : \sqrt{3} : 2$ , suggesting the microphase separation structure of PBA cylinder within LC matrix, with calculated  $d$ -spacing value of 15.0 nm. The lower LC content polymer (i.e., BC-77) exhibits primary scattering and its obscure higher order reflections in the ratio of 1:2. Combining AFM phase images, it can be concluded that a lamellar morphology with  $d$ -spacing value of 14.4 nm is formed. Meanwhile, polymers with even lower LC content (i.e., BC-67, BC-57, and BC-46) also form lamellar morphologies, similar to BC-77. For BC-33, primary scattering and its higher order reflections are in the ratio of  $1 : \sqrt{3} : 2$ , which suggests PCBOA cylinder within PBA matrix. The profiles of BC-25 have the scattering vector ratio of  $1:\sqrt{2}:\sqrt{3}:2$ , a characteristic of body-centered cubic structure with corresponding  $d$ -spacing of 22.8 nm.

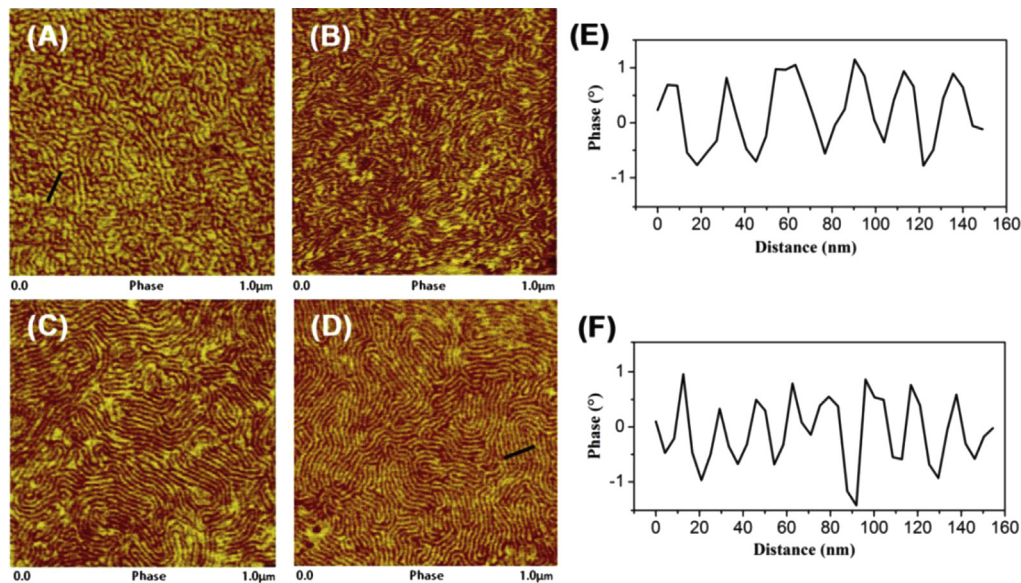
The phase diagram of PBA-*b*-PCBOA diblock copolymers is summarized in Fig. 3B. It's obvious that the lamellar morphology dominates during the majority LC block weight fraction range ( $f_{w,PCBOA} = 46\%–77\%$ ). Zhou et al. found that in rod–coil BCPs, the lamellar phase was observed with the supramolecular PMPCS rods aligning parallel to the lamellar normal [15]. Shen et al. reported that, for rod–coil BCPs, because long rods prefer a flat intermaterial dividing surface (IMDS), lamellar phases are stable in a wide range of composition even in some rod–coil BCPs with high compositional asymmetry [17]. Compared to those mesogen-jacketed rod–coil diblock copolymers, our block copolymers are similar to traditional side-chain LC copolymers where the smectic LC order contributes to stable lamellar structures [39].

Fig. 4 shows AFM phase images of the spin-coated and annealed films. The lighter and darker regions in the AFM images can be assigned to LC blocks and PBA blocks, respectively. As shown in Fig. 4A, a nonperiodic array of PBA spheres inside a continuous LC matrix was observed for BC-87. For BC-80, cylinders oriented parallel to the substrate were found in the films by combining with the SAXS results (Fig. 4B) [7,9,41–43]. Based on SAXS result, PBA cylinder-to-cylinder distance can be estimated as  $d_0 = 17.3$  nm [using  $d_0 = (4/3)^{1/2}d$ ], which is close to the  $d$ -spacing value of 17 nm estimated from AFM phase images. The lamellar morphology was observed obviously for BC-77 in Fig. 4C. The lamellar distance is

15 nm, close to 14.5 nm estimated from SAXS. Because PBA has low  $T_g$ , it's difficult to observe obvious phase images by AFM for BCPs with low LC contents, i.e., BC-25 for high viscosity of the sample. The AFM measurements can provide the surface morphology of polymers. However, this technique can hardly tell the underneath morphology due to its working method. For example, the laid down cylinder A in continuous B structure and the lamella A in lamella B structure should provide the similar AFM results [44–46]. In addition, for AFM measurement, the film thickness is usually around 100 nm. At this condition, the phase separation morphology in the film may be different as in the bulk [47]. Thus AFM results are usually used as a supplemental technique to better illustrate the phase separation morphology but not the critical data to determine the morphology. Usually, SAXS data are used as the crucial data to deduce the phase separation morphology from the higher ordered reflection peaks. In our case, SAXS data show clearly that BC-80 forms cylindrical morphology due to the ratio of scattering peak position in the order of  $1 : \sqrt{3} : 2$ , while BC-77 and BC-67 (Fig. 5D) form lamellar morphology due to the ratio of scattering peak position in the order of 1:2. As pointed above and in the mentioned references, the reason that BC-87 shows similar morphology as BC-67 is that the cylinders are laid down in the film, and provides similar results from AFM. The chain conformations of PCBOA segments, the phases of the PCBOA matrix, and the nanophase-separated structures of LCBCPs with different LC contents are schematically shown in Fig. 4D–F.

For the presence of LC block, lamellar morphology dominated the main range. It has been shown that the lamellar morphology can also stabilize LC phases. BCP thin films are of particular interest because of the possibility of obtaining two-dimensional patterns with very high regularity [47,48]. It is interesting to investigate how thermal annealing condition affects the microphase separation of BCP since the LC can promote the microphase separation of BCP.

The change of surface morphology from spin-coated BC-67 BCP thin films as a function of annealing time was investigated. After thermal annealing for 12 h and then slowly cooled to RT, an obvious lamellar morphology with average interlamellar spacing of 20 nm was observed, as shown in Fig. 5A. The continuity and ordering of self-assembled lamellar morphology are not satisfied for shorter annealing time. With increasing thermal annealing time, the



**Fig. 5.** AFM phase images of spin-coated BC-67 films on silicon substrates after annealing at 80 °C for different time. (A) 12 h, (B) 24 h, (C) 48 h and (D) 72 h. AFM phase profiles of A and D were shown in (E) and (F), respectively.

lamellar phase separation size reduced. When annealed for 72 h, the lamella phase separation size reduced to about 16 nm, as inferred through AFM imaging from the presence of a typical striped pattern (Fig. 5D and F). This phenomenon can be attributed to slow cooperative motion among mesomorphic units [49,50]. When annealed for enough time, self-assembly morphology induced by the formation of LC phase will develop to a better structure, that is an ordered lamellar structure with smaller interlamellar distance.

Furthermore, another thermal annealing condition can produce lamellar morphology with the smallest interlamellar spacing. For BC-67 after quenching from the isotropic phase to RT, a relatively disorder morphology was obtained, which is not a stable thermodynamic state of microphase-separated morphology. Fig. 6B shows the AFM image of BC-67 cooling slowly (0.4 °C min<sup>-1</sup>) from the isotropic phase to RT. It can be seen that the mesomorphic units have enough time and appropriate temperature to undergo LC cooperative motion, so the self-assembly morphology can develop well with interlamellar spacing of 14 nm, as shown in Fig. 6C. The possible reason is that the mesomorphic units align most closely during cooling process.

It's obvious that the mobility and phase behavior of LCBCPs may change the kinetic pathway of the self-assembly process in a supramolecular system. In-situ SAXS experiments were performed to determine the influence of temperature on the nanophase-separated structures of BC-77 and BC-67, as shown in Fig. 7.

The scattering vector positions of BC-77 annealed at different temperatures are almost the same within the range of errors (Fig. 7A). At temperatures higher than 100 °C, the lamellar reflection becomes less intense, suggesting an ODT. As the PCBOA blocks transform from the rod-like to the coil chain, the rearrangement of the polymer chains and the instability of microphase separation takes place during the transition process of the nanostructure. The isotropization temperature of BC-77 is nearly within experimental error of its ODT temperature. This correlation confirms our hypothesis that the isotropization of the LC domain can trigger the ODT [51]. This phenomenon can be explained on the basis of differences in smectic elastic free energies above and below the isotropization temperature.

For BC-67, when the temperature is increased to be higher than the 40 °C, a new peak with a higher  $q$  value appears in the ratio of 1:1.2 as shown in Fig. 7B, indicating the formation of a new structure. The strong first-order scattering vector,  $L$ , at  $q = 0.43 \text{ nm}^{-1}$  corresponds to a periodicity of 14.6 nm. The other, less intense reflections are due to the presence of cylinders and appear starting at  $q = 0.55 \text{ nm}^{-1}$  in a 1:2 scattering ratio of  $q$ , implying that the cylinders are arranged in a modified layer (ML) fashion [22,39]. The morphology is predominately lamellar with a small fraction contribution from cylinders. Upon cooling (see Fig. S4), the shoulder of the first-order  $L$  peak appears, thus confirming that at lower temperatures, dual L/ML morphology is one of thermal equilibrium.

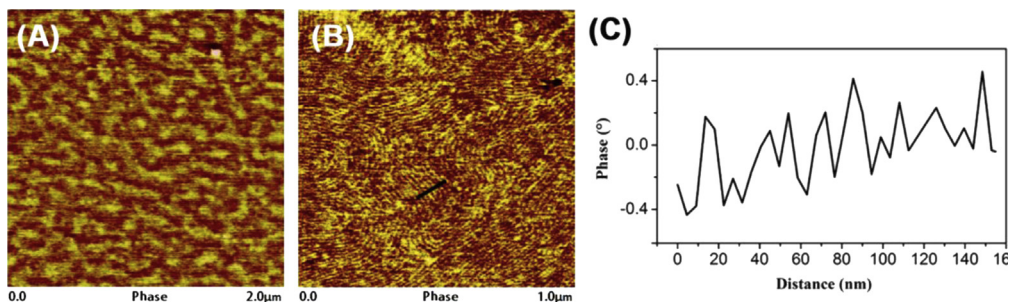


**Fig. 6.** AFM phase images of spin-coated BC-67 films on silicon substrates after annealing for different conditions: (A) at 140 °C above  $T_{150}$  for 2 h and quenched at RT, (B) at 140 °C above  $T_{150}$  for 2 h and slowly cooled (0.4 °C min<sup>-1</sup>) from the isotropic phase to the mesomorphic phase ( $T = 40$  °C). (C) AFM phase profiles of image B.

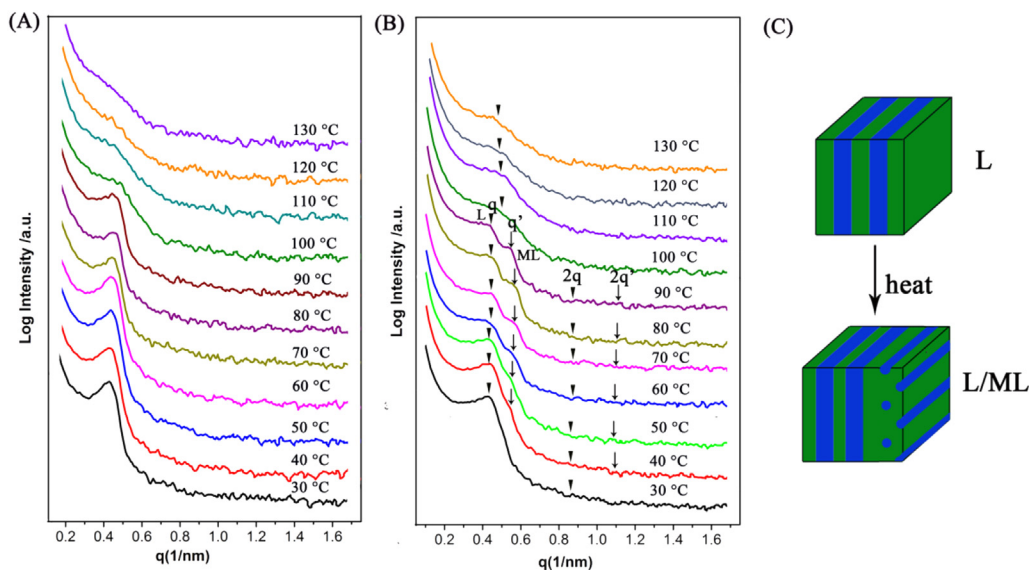


**Fig. 7.** Temperature-dependent 1D SAXS profiles of (A) BC-77, (B) BC-67 during heating. Data are plotted as the logarithm of the relative scattered intensity  $\log I(q)$  vs the scattering factor  $q$ . (C) Schematic model of order–order transition for BC-67. L: lamella, ML: modified layer.

This experiment proves that this sample undergoes a thermoreversible OOT at 30–90 °C from a purely lamellar morphology to a predominately lamellar morphology with cylindrical morphology, as shown in Fig. 7C. With further increase of temperature, the intensity of the diffraction peak of the new structure increases. As the temperature is further increased to above 100 °C, the diffraction peaks of the new structure disappear, and the intensities of diffraction peaks attributed to the lamellar reflection decrease, indicative of an ODT.

#### 4. Conclusions

In summary, we have successfully synthesized a series of well-defined diblock copolymers composed of amorphous PBA components and side-chain liquid crystalline PCBOA polymers with relative weight fraction of LC blocks varying from 25% to 87%. Combining SAXS and AFM, an intriguing microphase-separated suprastructure in correlation with mesophases as a function of  $f_{w,PCBOA}$  has been demonstrated. When the weight fraction of PCBOA is increased from 25% to 87%, PBA-spherical, PBA-cylindrical, lamella, LC-cylindrical and LC-spherical microphase separation structures were observed. The surface morphology change of spin-coated BC-67 BCP thin films with varying annealing time were also investigated. For spin-coated films, the size of lamellar phase separation structure decreased with increased thermal annealing time, while very slow cooling rate can lead to the lamella phase separation with the smallest spacing. Furthermore, the presence of LC blocks can trigger ODTs or OOTs of the nanophase-separated structures of BCPs: for BC-77, ODT was observed, while for BC-67, a thermoreversible OOT, lamella to lamella/modified layer (L/ML) was observed.

#### Acknowledgments

The financial support from the National Natural Science Foundation of China (No. 21104050), China Postdoctoral Science Foundation (2013M541715, 2014T70541), a Project Funded by the Priority Academic Program Development of Jiangsu Higher Education Institutions is gratefully acknowledged.

#### Appendix A. Supplementary data

Supplementary data related to this article can be found at <http://dx.doi.org/10.1016/j.polymer.2015.01.077>.

#### References

- [1] Kim JK, Yang SY, Lee Y, Kim Y. *Prog Polym Sci* 2010;35:1325–49.
- [2] Darling SB. *Prog Polym Sci* 2007;32:1152–204.
- [3] Lee M, Cho BK, Zin WC. *Chem Rev* 2001;101:3869–92.
- [4] Zhu Y, Zhou YQ, Chen Z, Lin R, Wang XG. *Polymer* 2012;53:5666–76.
- [5] Shi LY, Pan Y, Zhang QK. *Chin J Polym Sci* 2014;32:1524–34.
- [6] Hajduk DA, Harper PE, Gruner SM, Honeker CC, Kim G, Thomas EL, et al. *Macromolecules* 1994;27:4063–75.
- [7] Yu HF, Naka Y, Shishido A, Ikeda T. *Macromolecules* 2008;41:7959–66.
- [8] Matsen MW, Schick M. *Macromolecules* 1994;27:4014–5.
- [9] Yu HF, Kobayashi T. *ACS Appl Mater Interfaces* 2009;1:2755–62.
- [10] Bates FS, Schulz MF, Khandpur AK, Forster S, Rosedale JH, Almdal K, et al. *Faraday Discuss* 1994;98:7–18.
- [11] Wei W, Liu Y, Xiong HM. *Polymer* 2013;54:6793–800.
- [12] Olsen BD, Segalman RA. *Macromolecules* 2007;40:6922–9.
- [13] Olsen BD, Shah M, Ganesan V, Segalman RA. *Macromolecules* 2008;41:6809–17.
- [14] Muthukumar M, Ober CK, Thomas EL. *Science* 1997;277:1225–32.
- [15] Tenneti KK, Chen XF, Li CY, Tu YF, Wan XH, Zhou QF, et al. *J Am Chem Soc* 2005;127:15481–90.
- [16] Berg GJ, McBride MK, Wang C, Bowman CN. *Polymer* 2014;55:5849–72.
- [17] Shi LY, Zhou Y, Fan XH, Shen ZH. *Macromolecules* 2013;46:5308–16.
- [18] Schneider A, Zanna JJ, Yamada M, Finkelmann H, Thomann R. *Macromolecules* 2000;33:649–51.
- [19] Sanger J, Gronski W, Maas S, Stuhn B, Heck B. *Macromolecules* 1997;30:6783–7.
- [20] Zheng WY, Hammond PT. *Macromolecules* 1998;31:711–21.
- [21] Guan Y, ChenX Ma H, Shen Z, Wan X. *Soft Matter* 2010;6:922–7.
- [22] Anthamatten M, Zheng WY, Hammond PT. *Macromolecules* 1999;32:4838–48.
- [23] Verploegen E, McAfee LC, Tian LT, Verploegen D, Hammond PT. *Macromolecules* 2007;40:777–80.
- [24] Osuji CO, Chen JT, Mao G, Ober CK, Thomas EL. *Polymer* 2000;41:8897–907.
- [25] Palyulin VV, Potemkin II. *J Chem Phys* 2007;127:124903.
- [26] Potemkin II, Bodrova AS. *Macromolecules* 2009;42:2817–25.
- [27] Verploegen E, Zhang TJ, Jung YS, Ross C, Hammond PT. *Nano Lett* 2008;8:3434–40.
- [28] Kasko AM, Grunwald SR, Pugh C. *Macromolecules* 2002;35:5466–74.
- [29] Kasko AM, Heintz AM, Pugh C. *Macromolecules* 1998;31:256–71.
- [30] Min B, Kim SH, Namgoong H, Kwon SH. *Polym Bull* 1999;42:587–94.
- [31] Xu QZ, Chen JY, Huang WC, Li YW, Yang XM, Tu YF, et al. *Macromolecules* 2013;46:7274–81.
- [32] Huang WC, Wan YB, Li XH, Yang XM, Li YW, Tu YF, et al. *Polym Chem* 2014;5:945–54.

- [33] Kurihara S, Ikeda T, Tazuke S. *Macromolecules* 1993;26:1590–4.
- [34] Kostromin SG, Shibaev VP. *Makromol Chem Phys* 1990;191:2521–7.
- [35] Fischer H, Poser S, Arnold M. *Macromolecules* 1996;28:6957–62.
- [36] Tian YQ, Watanabe K, Kong XX, Abe J, Iyoda T. *Macromolecules* 2002;35:3739–47.
- [37] Nardele CG, Asha SK. *J Phys Chem B* 2014;118:1670–84.
- [38] Gray GW, Goodby JW. *Smectic liquid crystals—textures and structures*. London: Leonard Hill; 1984.
- [39] Anthamatten M, Hammond PT. *Macromolecules* 1999;32:8066–76.
- [40] Takeshita H, Taniguchi S, Arimoto M, Miya M, Takenaka K, Shiomi T. *Polymer* 2009;50:271–8.
- [41] Yu HF, Li JZ, Ikeda T, Iyoda T. *Adv Mater* 2006;18:2213–5.
- [42] Dong J, Zhang RC, Zhan XW, Yang H, Zhu SQ, Wang GJ. *Prog Polym Sci* 2014;39:781–815.
- [43] Morikawa Y, Kondo T, Nagano S, Seki T. *Chem Mater* 2007;19:1540–2.
- [44] Kim E, Ahn H, Park S, Lee H, Lee M, Ryu DY. *ACS Nano* 2013;7:1952–60.
- [45] Campbell IP, He C, Stoykovich MP. *ACS Macro Lett* 2013;2:918–23.
- [46] Gong J, Ahn H, Kim E, Lee H, Park S, Ryu DY. *Soft Matter* 2012;8:3570–5.
- [47] Zhang XH, Douglas JF, Jones RL. *Soft Matter* 2012;8:4980–7.
- [48] King A, Presnall D, Steely LB, Allcock HR, Wynne KJ. *Polymer* 2013;54:1123–9.
- [49] Yu HF, Kobayashi T, Yang H. *Adv Mater* 2011;23:3337–44.
- [50] Yu HF, Asaoka S, Shishido A, Iyoda T, Ikeda T. *Small* 2007;3:768–71.
- [51] Yamada M, Iguchi T, Hirao A, Nakahama S, Watanabe J. *Polym J* 1998;30:23–30.